Supplements to "Nonparametric Interrogation of Transcriptional Regulation in Single-Cell RNA and Chromatin Accessibility Multiomic Data"

Yuriko Harigaya[1], Zhaojun Zhang[2], Hongpan Zhang[3,4], Chongzhi Zang[3,4,5], Nancy R Zhang[2,*], Yuchao Jiang[6,7,8,*]

1 Curriculum in Bioinformatics and Computational Biology, School of Medicine, University of North Carolina, Chapel Hill, NC 27599, USA.
2 Department of Statistics, The Wharton School, University of Pennsylvania, Philadelphia, PA 19104, USA.
3 Center for Public Health Genomics, University of Virginia, Charlottesville, VA 22908, USA.
4 Department of Biochemistry and Molecular Genetics, University of Virginia, Charlottesville, VA 22908, USA.
5 Department of Public Health Sciences, University of Virginia, Charlottesville, VA 22908, USA.
6 Lineberger Comprehensive Cancer Center, University of North Carolina at Chapel Hill, NC 27599, USA.
7 Department of Genetics, School of Medicine, University of North Carolina, Chapel Hill, NC 27599, USA.
8 Department of Biostatistics, Gillings School of Global Public Health, University of North Carolina, Chapel Hill, NC 27599, USA.

To whom correspondence should be addressed: nzh@wharton.upenn.edu, yuchaoj@email.unc.edu.

Supplementary Figures

Supplementary Fig. 1 | Reduced dimensions for single-cell multiomic datasets. a-c, UMAP[1] embedding of single cells for the 10X Genomics PBMC, 10X Genomics mouse embryonic brain, and SHARE-seq[2] mouse skin. The three columns show UMAP embedding based on RNA, ATAC, and WNN[3], respectively, with colors corresponding to transferred/inferred cell types. The last column shows the UMAP embedding overlaid with metacell assignments.

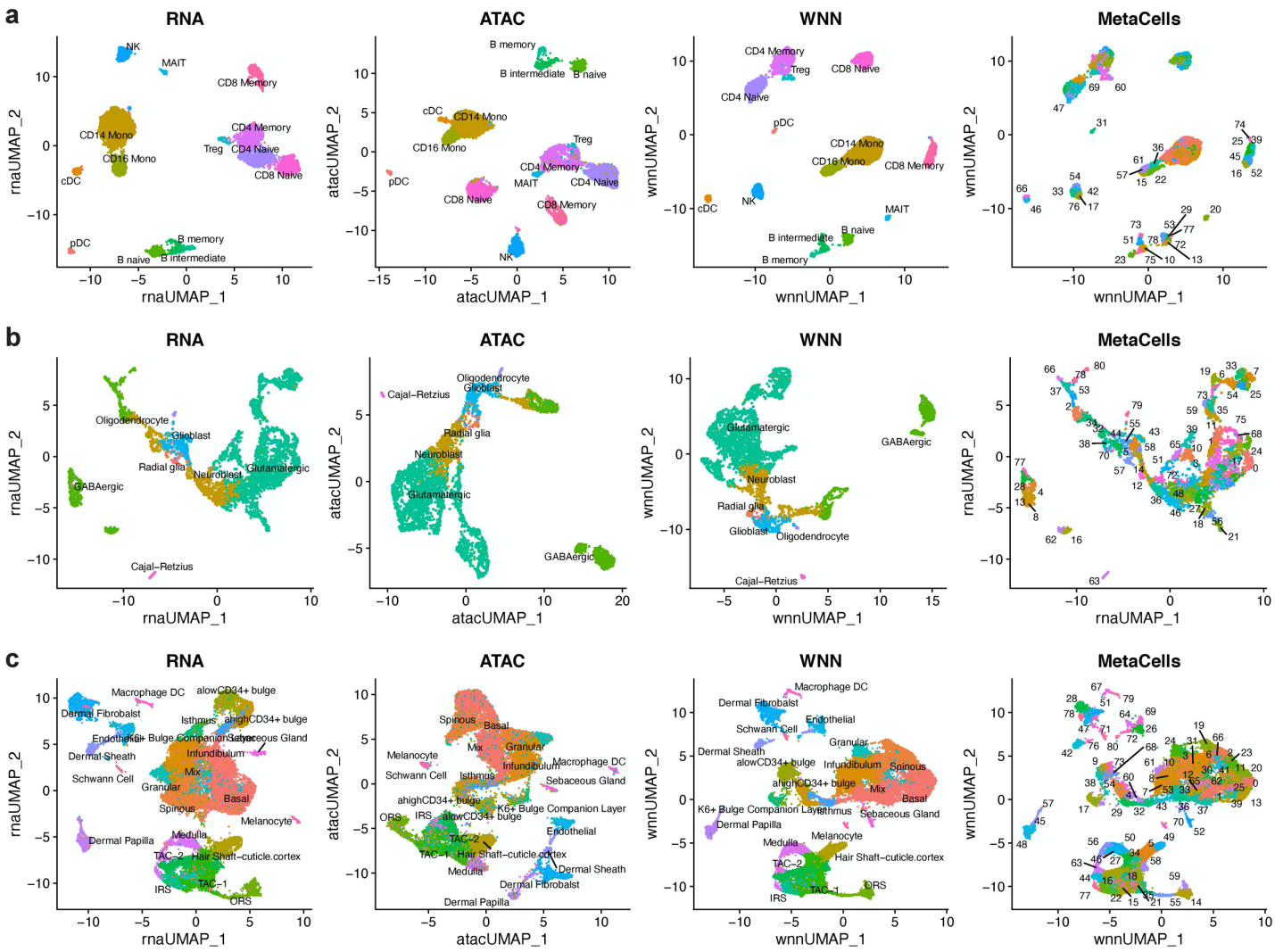

Supplementary Fig. 2 | Reduced dimensions and RNA prediction for SNARE-seq adult mouse brain data[4]. a, UMAP embedding of single cells based on RNA, ATAC, and WNN, respectively. **b**, Box plots showing distributions of Pearson correlations between observed and predicted RNA expression levels across top 1000 highly variable genes. The horizontal axis represents the sizes of the windows centered at TSSs.

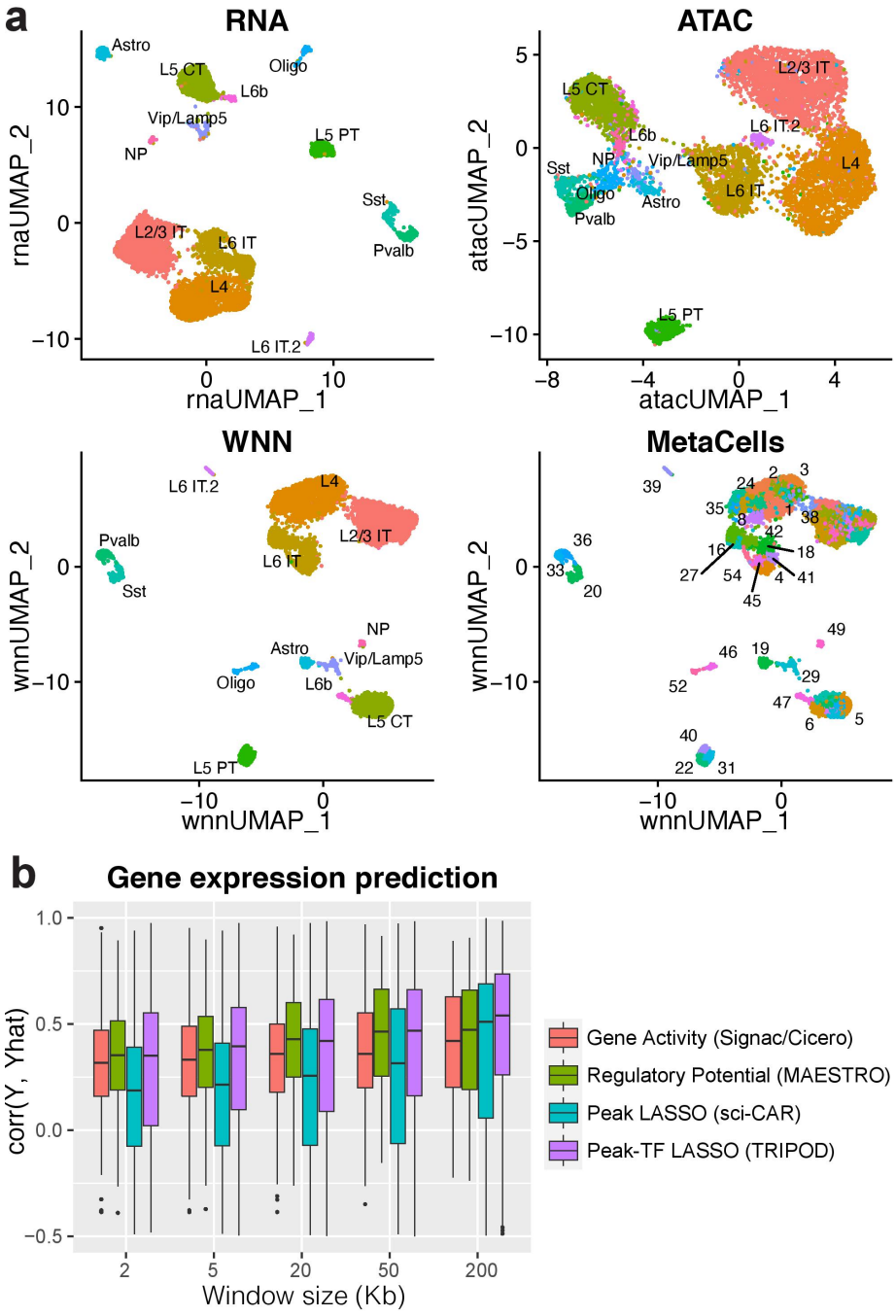

Supplementary Fig. 3 | RNA prediction using independent training and testing datasets of PBMC. We trained the supervised prediction model using the dataset of 10k PBMCs, adopted an independent single-cell multiomic dataset of 3k PBMCs as a testing dataset. We merged the two datasets to align genes, peaks, and TFs, and showed that the peak-TF LASSO model significantly increases the prediction accuracy. Distributions of Pearson correlations between observed and predicted RNA expression levels from the testing dataset are shown.

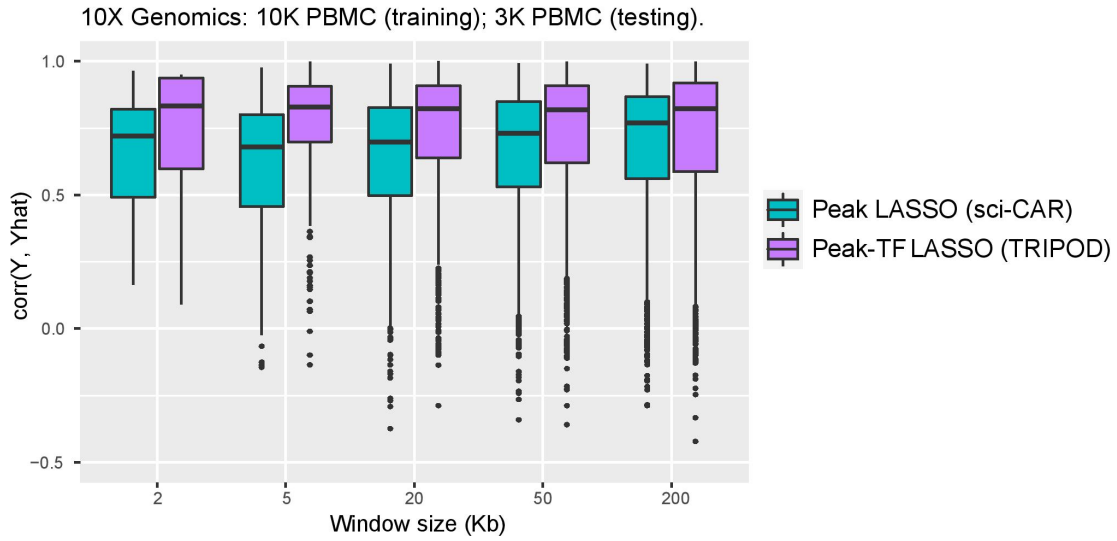

Supplementary Fig. 4 | RNA and ATAC coverage across different single-cell multiomic sequencing protocols. TRIPOD was applied to the 10X PBMC, 10X mouse embryonic brain, and SHARE-seq mouse skin data to detect regulatory trios. Data from SNARE-seq[4] and PAIRED-seq[5] suffer from low sequencing depth.

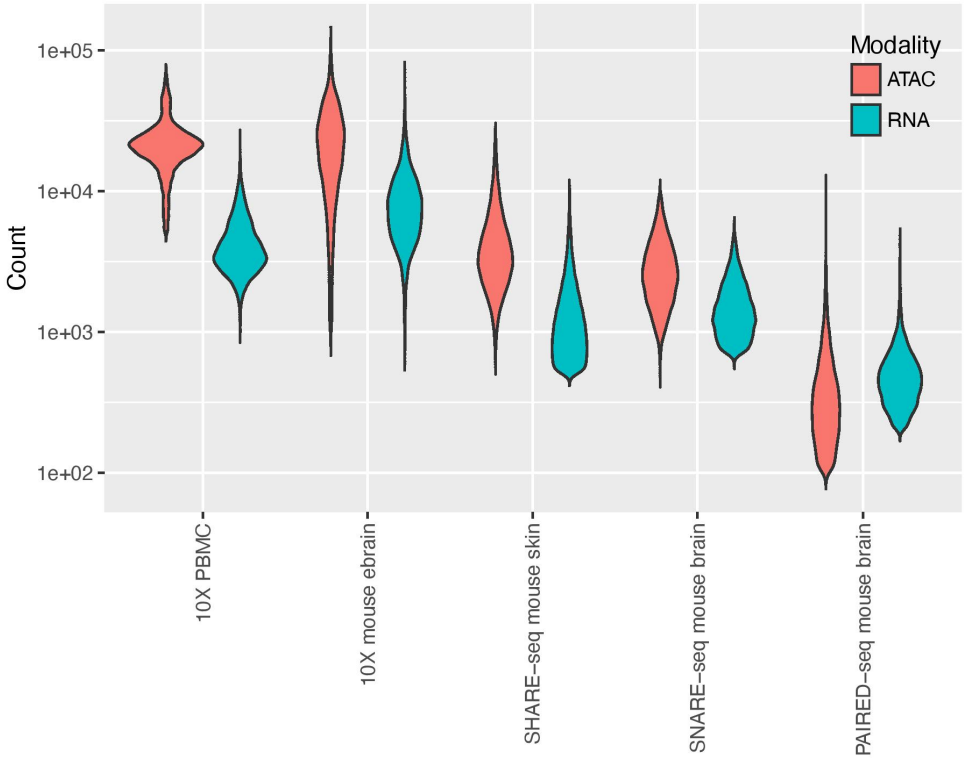

Supplementary Fig. 5 | Summary statistics of peaks, genes, and motifs in the PBMC data. a, Histograms of the number of peaks within regions of 100kb/200kb up and downstream of genes' TSSs. **b**, Histograms of the number of genes within regions of 100kb/200kb up and downstream of genes' TSSs. **c**, Histogram of the number of motifs per peak. Of the many possible and biologically meaningful peak-TF-gene combinations, TRIPOD proceeds to scan for trios with significant conditional associations.

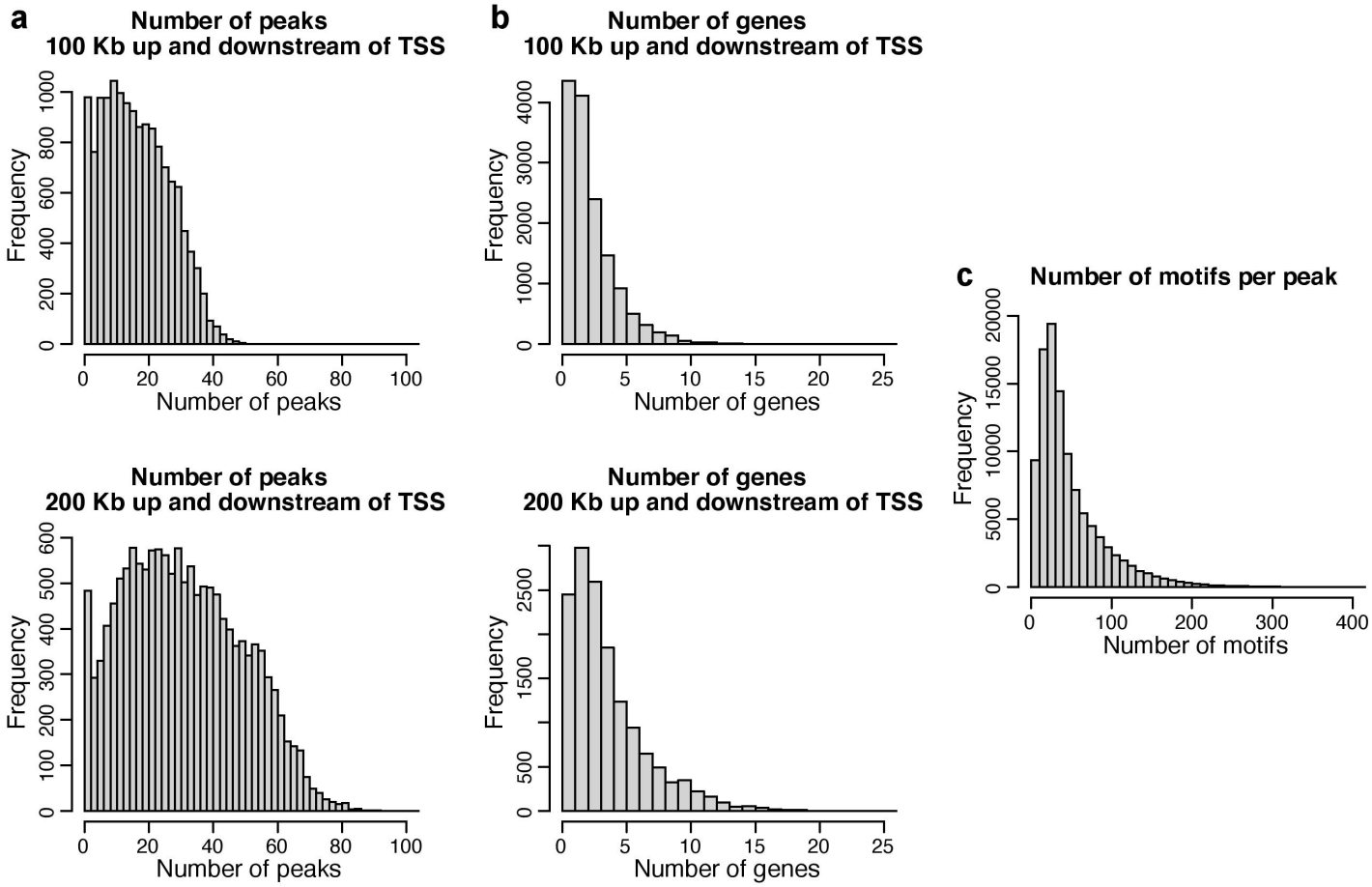

Supplementary Fig. 6 | Regulatory relationships identified by LinkPeaks, marginal association, and TRIPOD in the PBMC data. a, Venn diagrams of the number of peak-gene pairs captured by LinkPeaks[6], marginal association between gene expression and peak accessibility, and TRIPOD for representative target genes (*CCR7*, *GNLY*, *FCGR3A*, and *MS4A1*). For TRIPOD, the union set between level 1 and level 2 testing matching by TF expression is shown. **b**, Venn diagrams of the number of TF-gene pairs captured by marginal association between gene expression and TF expression and TRIPOD. For TRIPOD, the union set between level 1 and level 2 testing matching by peak accessibility is shown. TRIPOD complements and contrasts with existing methods based on marginal associations.

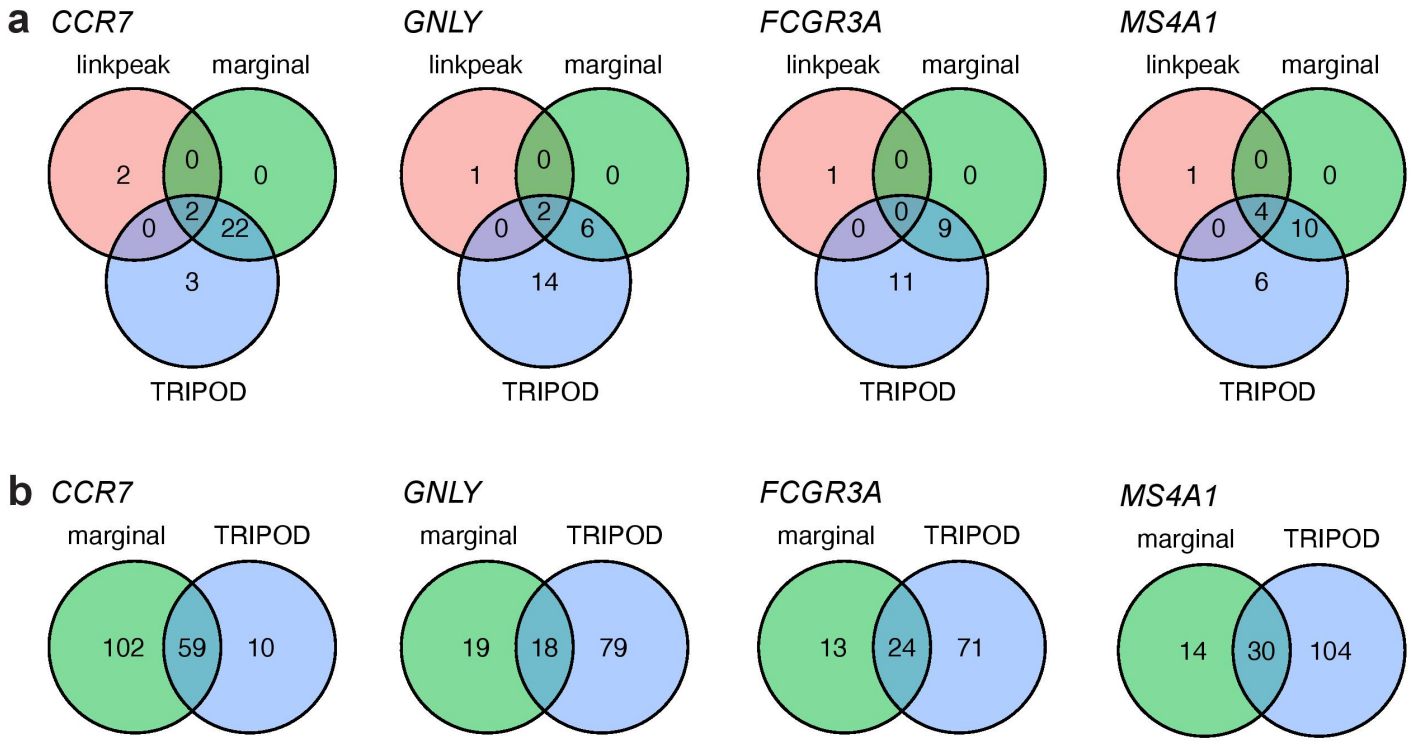

Supplementary Fig. 7 | Identification of putative cell-type-specific trio regulatory relationships in PBMC. Results from cell-type-specific influence analyses are shown for the same example trios as in Fig. 3a,b. **a**, Metacell-specific Cook's distance. **b**, Metacell-specific DFFITS. **c**, Cell-type-specific influential p-values. **d**, Cell-type hierarchies constructed from the RNA domain using highly variable genes. Red/gray circles indicate whether removal of the corresponding branches of metacells significantly changes the model fitting; crosses indicate that removal of the groups of metacells resulted in inestimable coefficients. **e**, Cell-type-specific DNA footprinting signatures of the TF binding motifs. The enrichment results supported the key regulatory cell types identified from the influence analyses.

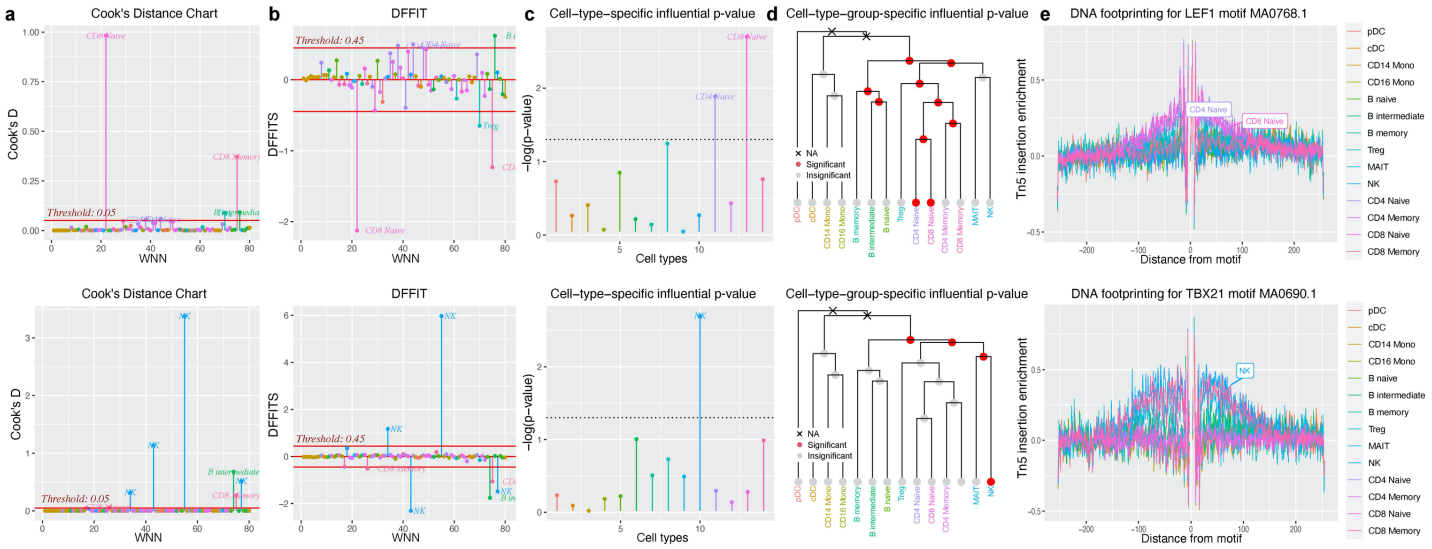

Supplementary Fig. 8 | Trio regulatory relationships identified by LinkPeaks, marginal association, and TRIPOD, and validation thereof using PLAC-seq data. a, Bar plots of the numbers of significant regulatory links detected by TRIPOD and marginal associations. The numbers of peak-gene pairs and TF-gene pairs were obtained by collapsing trios by TFs and peaks, respectively. **b**, Heatmap showing the degree of enrichment of ATAC peaks in enhancer-promoter contacts by PLAC-seq[5]. **c**, Venn diagrams of the number of peak-gene pairs captured by PLAC-seq, marginal association between gene expression and peak accessibility, and various models as indicated on the top of each diagram.

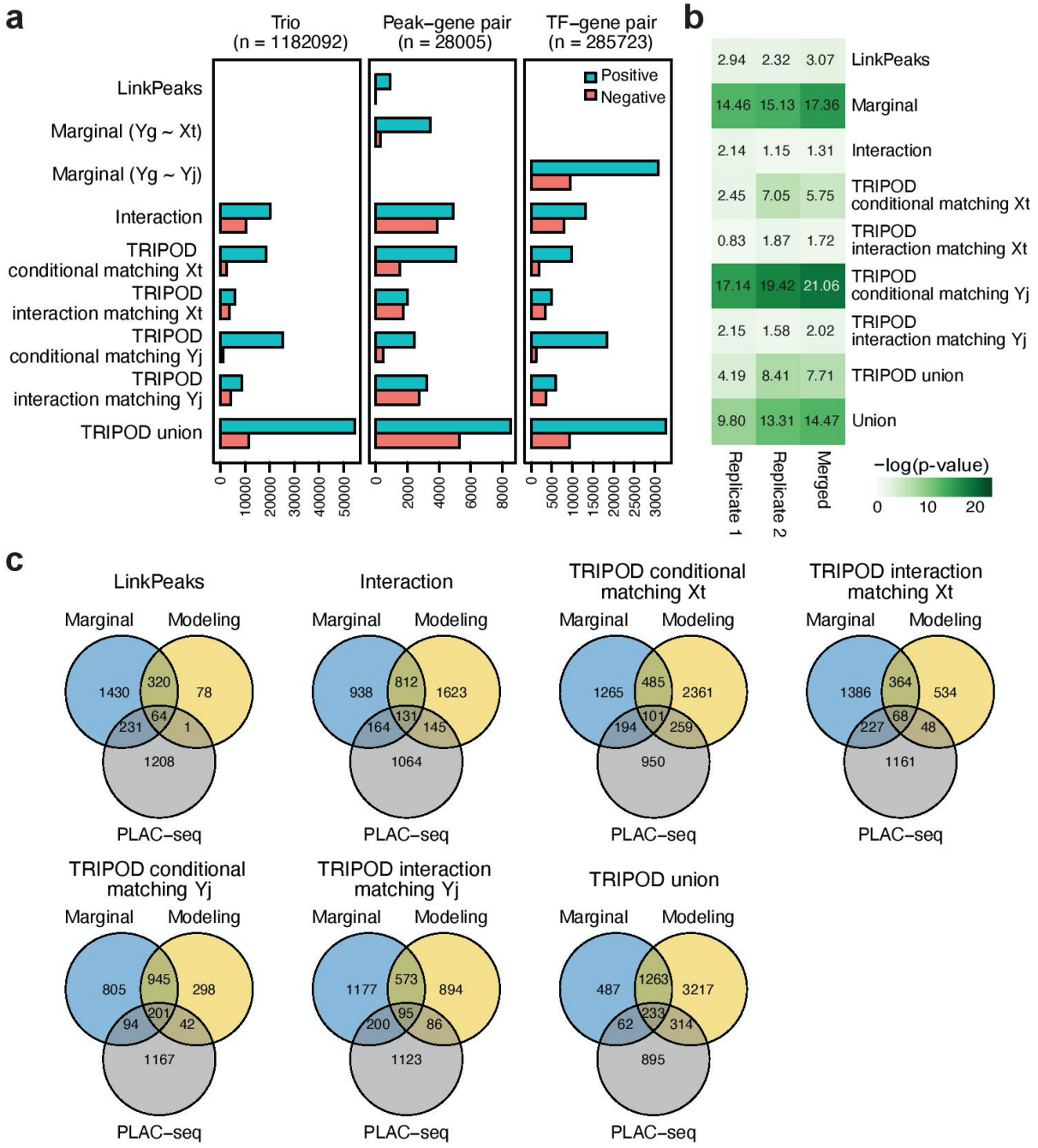

Supplementary Fig. 9 | Visualization of regulatory links representing possible crosstalks between neurogenesis- and gliogenesis-specific TF cascades. a, Putative regulation of *Nfia* by Neurog2, Eomes, and Tbr1. **b**, Putative regulation of *Sox9* by Neurog2. ChIP-seq peaks for the indicated TFs are included; arcs represent significant regulatory links inferred by TRIPOD.

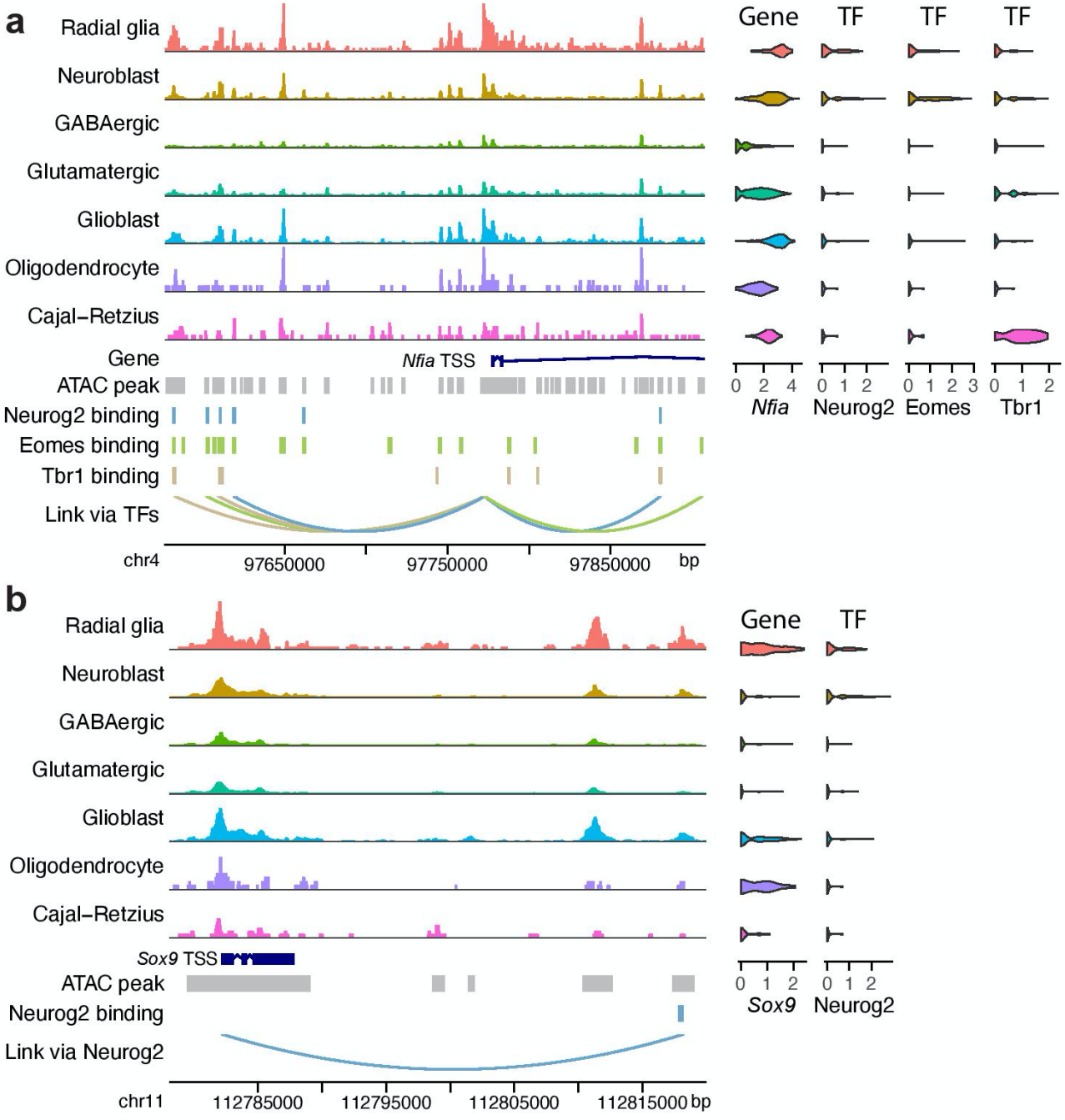

Supplementary Fig. 10 | Identification of putative cell-type- and cell-state-specific regulation in mouse embryonic brain. a-h, Visualization of eight example trios from the neurogenesis and gliogenesis TF cascades. The scatter plots (left) show TRIPOD's modeling fitting; the points represent metacells and are colored based on cell types. The middle panels show cell-type-specific p-values from the sampling-based influence analyses. The colors on the UMAP embedding (right) correspond to the smoothed p-values from the sampling-based influence analyses along the differentiation trajectory. Genomic coordinates for the peaks are from mm10.

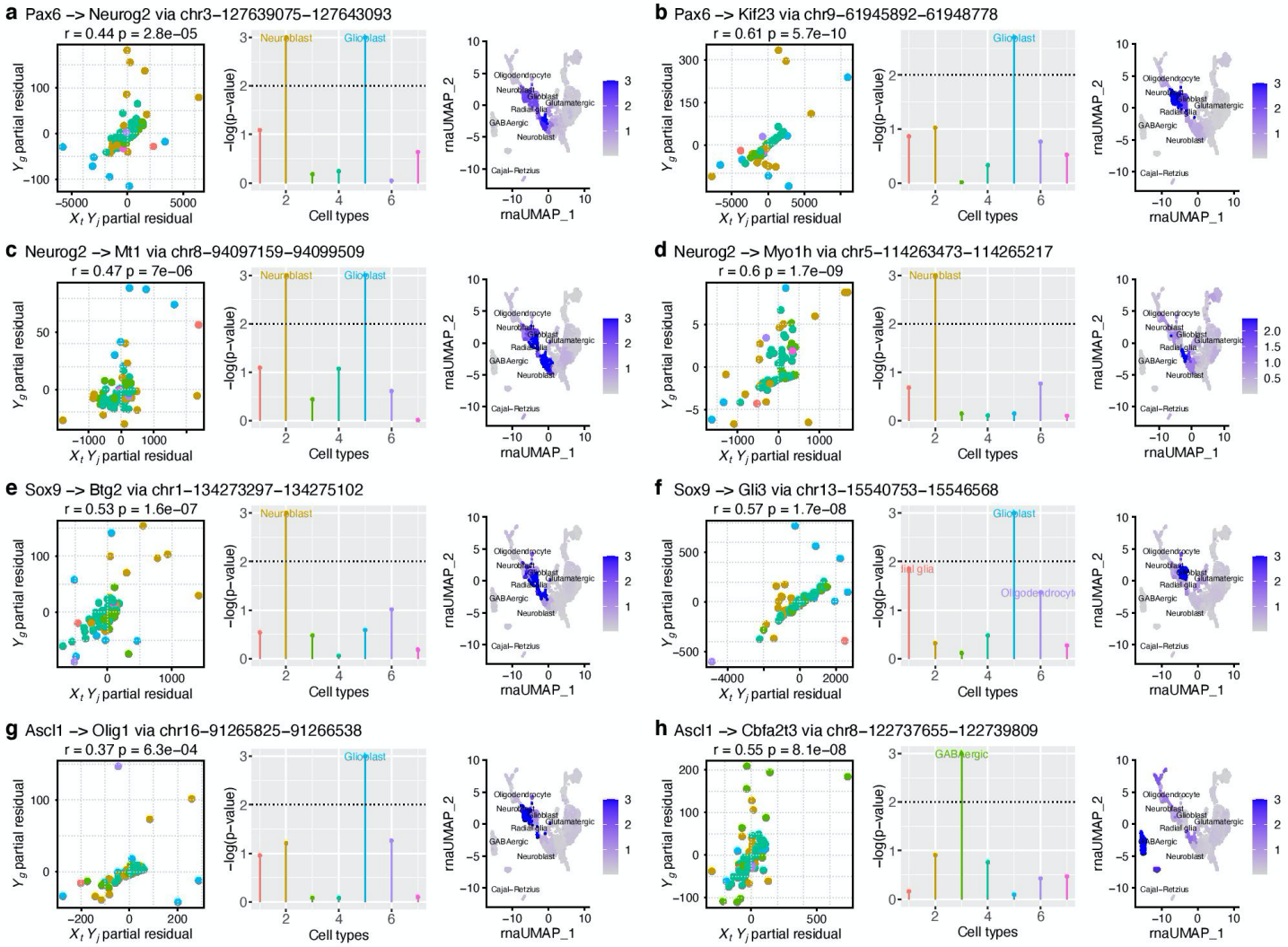

Supplementary Fig. 11 | Assessing linear models for detecting conditional associations. Scatter plots comparing fittings from linear models and TRIPOD's level 1 and level 2 testing for example trios in **a**, PBMC and **b**, mouse skin. Genomic coordinates for the peaks are from hg38 for human and mm10 for mouse.

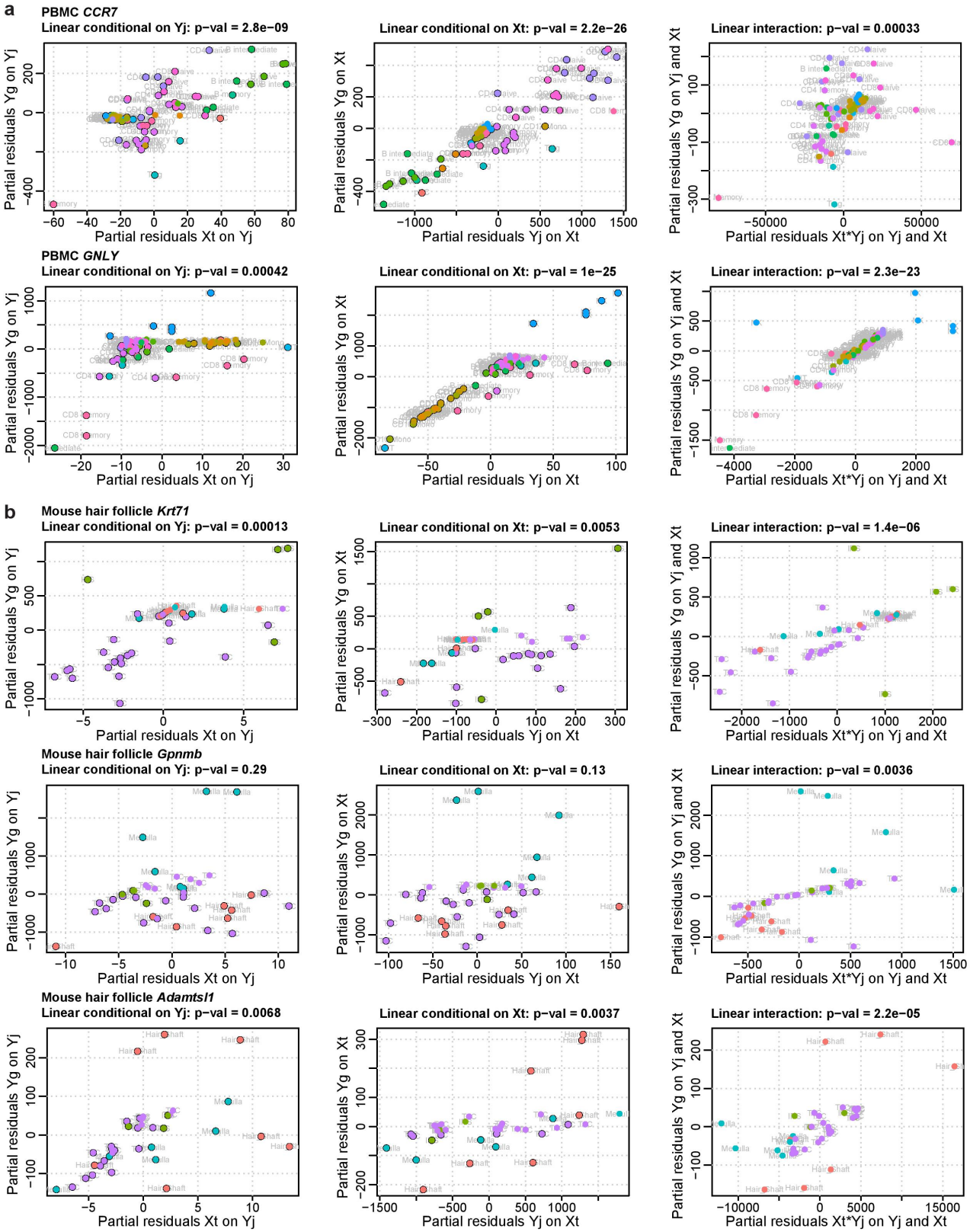

Supplementary Fig. 12 | Comparison of estimated coefficients from linear model and TRIPOD'S nonparametric model. a-d, Pairwise scatter plots comparing transformed coefficients from linear model and TRIPOD's nonparametric model for representative target genes, *CCR7*, *GNLY*, *FCGR3A*, and *MS4A1* from the PBMC data. γ denotes the coefficient for the interaction between TF expression and peak accessibility; α and β denote the coefficients for the partial gene-peak and gene-TF correlations, respectively. The three coefficients are fit using the linear model and TRIPOD's level 1 and level 2 testing, and their estimates are correlated on the global scale. However, the actual call sets are different, and the underlying models and assumptions are different.

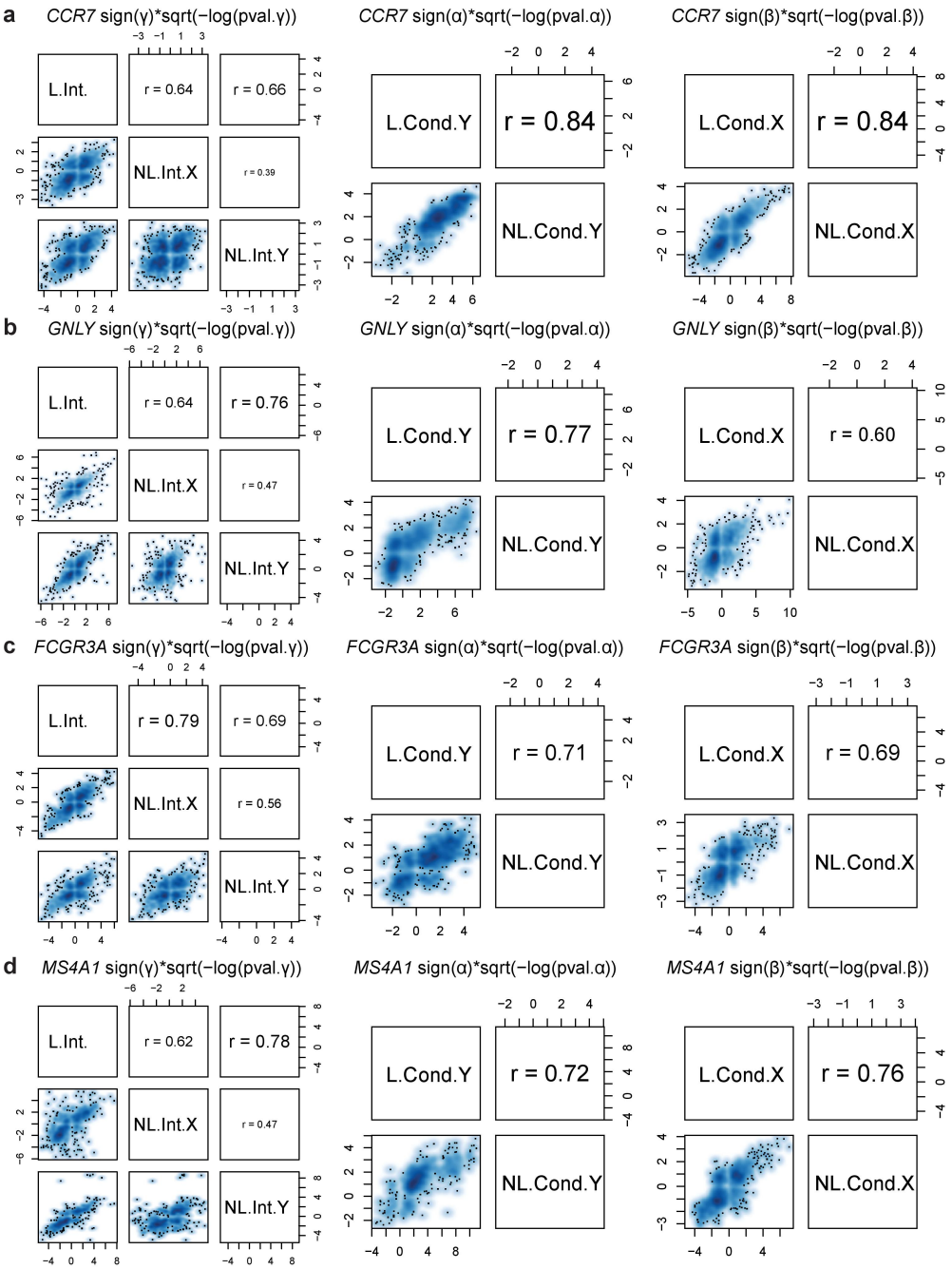

Supplementary Fig. 13 | Comparison of the trio regulatory relationships identified by linear model and TRIPOD's nonparametric model. a-d, Venn diagrams of the number of significant trios detected by linear and TRIPOD models for representative target genes, *CCR7*, *GNLY*, *FCGR3A*, and *MS4A1*. The left, middle, and right panels contain results from the interaction models, the models conditional on TF expression Y_j, and the models conditional on peak accessibility X_t. L.int., TRIPOD.Int.Y, TRIPOD.Int.X, L.Cond.Y, TRIPOD.Cond.Y, L.Cond.X, and TRIPOD.Cond.X represent linear interaction model, nonparametric interaction model matching by TF expression (TRIPOD level 2 test), nonparametric interaction model matching by peak accessibility (TRIPOD level 2 test), linear model conditional on TF expression, nonparametric conditional model matching by TF expression (TRIPOD level 1 test), linear model conditional on peak accessibility, and nonparametric conditional model matching by peak accessibility (TRIPOD level 1 test), respectively.

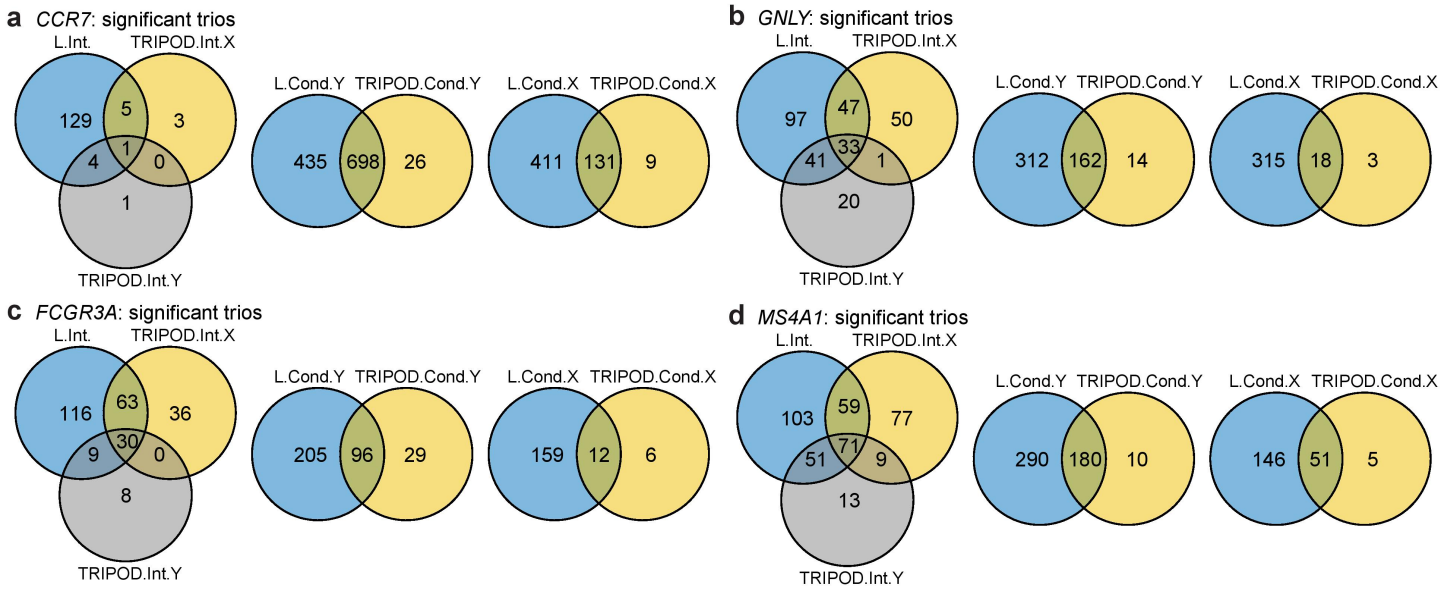

Supplementary Tables

Supplementary Table 1 | Single-cell RNA and ATAC multiomic datasets. Data adopted in this study from different tissues, organisms, and cell types using different protocols are summarized. The number of cells, peaks, and genes, as well as RNA read counts and ATAC read counts **a**, before and **b**, after quality control (QC) are summarized. Sources of data are also provided.

(A)

Organism	Tissue	Protocol	PMID or source	Before QC				
				Number of cells	Number of peaks	Number of genes	Mean cov. ATAC	Mean cov. RNA
Homo sapiens	PBMC	10X Genomics Multiome	10X Genomics	11909	108377	36601	20434	4402
Homo sapiens	PBMC	10X Genomics Multiome	10X Genomics	2714	156607	36601	20661	4344
Mus musculus	Embryonic brain at day 18	10X Genomics Multiome	10X Genomics	4881	139083	32285	20989	9486
Mus musculus	Skin late anagen	SHARE-seq	33098772	34774	344592	23296	4231	1259
Mus musculus	Adult brain cerebral cortex	SNARE-seq	31611697	10309	244544	33160	2656	1549
Mus musculus	Adult brain cerebral cortex	PAIRED-seq	31695190	15191	2614863	29624	1600	459

(B)

Organism	Tissue	Protocol	PMID or source	After QC				
				Number of cells	Number of peaks	Number of genes	Mean cov. ATAC	Mean cov. RNA
Homo sapiens	PBMC	10X Genomics Multiome	10X Genomics	7790	103755	14508	9611	3352
Homo sapiens	PBMC	10X Genomics Multiome	10X Genomics	2206	106056	36601	13534	4425
Mus musculus	Embryonic brain at day 18	10X Genomics Multiome	10X Genomics	3962	139083	14476	12520	8293
Mus musculus	Skin late anagen	SHARE-seq	33098772	29308	343783	15086	17886	1080
Mus musculus	Adult brain cerebral cortex	SNARE-seq	31611697	7533	244544	15332	12534	2053
Mus musculus	Adult brain cerebral cortex	PAIRED-seq	31695190	11292	118337	17858	3014	387

Supplementary Table 2 | ChIP-seq data of human blood (B lymphocyte, T lymphocyte, and monocyte). Non-cancerous and cell-type-specific ChIP-seq data of human blood were downloaded from the Cistrome[7] portal to validate the peak-TF links in the PBMC single-cell multiomic data. PCR bottleneck coefficient (PBC) is used to estimate the rate of read duplication through PCR amplification; a good PBC score is ≥ 80%. PeaksFoldChangeAbove10 contains the number of peaks called by MACS2[8] with a fold change above 10. FRiP is used for evaluating the signal-to-noise ratio; a good FRiP score is ≥ 1%. PeaksUnionDHSRatio is the percentage of the merged top 5000 peaks (ordered by MACS2 q-value) that overlap with union DHS regions; this is expected to be ≥ 70%.

DCid	Species	GSMID	Factor	Cell_line	Cell_type	Tissue_type	FastQC	UniquelyMappedRatio	PBC	PeaksFoldChangeAbove10	FRiP	PeaksUnionDHSRatio
40022	Homo sapiens	GSM1121094	BRD4	None	B Lymphocyte	Blood	38	0.8193	0.955	1615	0.1565535	0.9436
40053	Homo sapiens	GSM1121098	CDK7	None	B Lymphocyte	Blood	38	0.7267	0.962	1230	0.05939275	0.9608
40226	Homo sapiens	GSM1195559	CDK9	None	B Lymphocyte	Blood	38	0.7745	0.937	4517	0.09261	0.9696
45178	Homo sapiens	GSM1003474	CTCF	None	B Lymphocyte	Blood	38	0.7908	0.904	27265	0.305596	0.9758
45179	Homo sapiens	GSM1003476	H2AZ	None	B Lymphocyte	Blood	37	0.7298	0.94	2524	0.1956965	0.975
40215	Homo sapiens	GSM1195560	IRF4	None	B Lymphocyte	Blood	38	0.8383	0.948	8535	0.13387325	0.9422
40216	Homo sapiens	GSM1195557	MED1	None	B Lymphocyte	Blood	38	0.5248	0.844	4058	0.14310625	0.9664
40233	Homo sapiens	GSM1195555	MED1	None	B Lymphocyte	Blood	38	0.6613	0.911	9273	0.2180545	0.954
40234	Homo sapiens	GSM1195556	MED1	None	B Lymphocyte	Blood	38	0.8217	0.963	4479	0.1278495	0.9472
5967	Homo sapiens	GSM762709	MYC	None	B Lymphocyte	Blood	29	0.7391	0.988	1211	0.048873002	0.9576
33439	Homo sapiens	GSM971344	POLR2A	None	B Lymphocyte	Blood	30	0.7135	0.922	4948	0.1402875	0.9746
33434	Homo sapiens	GSM971343	SMARCA4	None	B Lymphocyte	Blood	30	0.6431	0.909	2353	0.0451365	0.964
45444	Homo sapiens	GSM1003508	CTCF	None	Monocyte	Blood	37	0.7086	0.948	23384	0.243658	0.9718
45441	Homo sapiens	GSM1003548	H2AZ	None	Monocyte	Blood	37	0.8274	0.898	1674	0.11932275	0.975
41301	Homo sapiens	GSM1057025	IRF1	None	Monocyte	Blood	38	0.8155	0.932	11224	0.07846625	0.9264
41302	Homo sapiens	GSM1057026	IRF1	None	Monocyte	Blood	38	0.8212	0.943	3018	0.028401	0.945
41303	Homo sapiens	GSM1057027	IRF1	None	Monocyte	Blood	38	0.8198	0.877	5920	0.04798775	0.9316
81223	Homo sapiens	GSM2687534	RUNX1	None	Monocyte	Blood	38	0.7012	0.919	9496	0.31398225	0.9418
85986	Homo sapiens	GSM2804465	SPI1	None	Monocyte	Blood	39	0.7064	0.944	1283	0.038436584	0.9426
41287	Homo sapiens	GSM1057011	STAT1	None	Monocyte	Blood	39	0.8088	0.993	6006	0.11584575	0.976
41288	Homo sapiens	GSM1057012	STAT1	None	Monocyte	Blood	39	0.7591	0.995	1501	0.0587395	0.9728
41289	Homo sapiens	GSM1057013	STAT1	None	Monocyte	Blood	39	0.8118	0.993	11395	0.15686975	0.9774
82662	Homo sapiens	GSM2679938	T	None	Monocyte	Blood	39	0.8392	0.992	11428	0.14325775	0.9586
81224	Homo sapiens	GSM2687535	TET2	None	Monocyte	Blood	38	0.6452	0.79	2851	0.22890725	0.7862
36301	Homo sapiens	GSM823379	BRD4	None	T Lymphocyte	Blood	39	0.6184	0.803	1025	0.02953575	0.9652
38389	Homo sapiens	GSM1022944	BRD4	None	T Lymphocyte	Blood	38	0.7591	0.968	1092	0.04322775	0.9644
3060	Homo sapiens	GSM325895	CTCF	None	T Lymphocyte	Blood	29	0.5214	0.902	15633	0.253560996	0.9716
44090	Homo sapiens	GSM1056928	ETS1	None	T Lymphocyte	Blood	37	0.5843	0.965	1319	0.0132305	0.96
44092	Homo sapiens	GSM1056930	ETS1	None	T Lymphocyte	Blood	39	0.803	0.909	3052	0.0402015	0.9594
44093	Homo sapiens	GSM1056931	ETS1	None	T Lymphocyte	Blood	38	0.7048	0.905	1559	0.02145925	0.956
44094	Homo sapiens	GSM1056932	ETS1	None	T Lymphocyte	Blood	39	0.7582	0.903	2587	0.039202	0.9608
4459	Homo sapiens	GSM393968	POLR2A	None	T Lymphocyte	Blood	27	0.5922	0.982	3068	0.04810575	0.972
36302	Homo sapiens	GSM823380	POLR2A	None	T Lymphocyte	Blood	39	0.7371	0.8	10180	0.2364385	0.9728
38342	Homo sapiens	GSM1022949	POLR2A	None	T Lymphocyte	Blood	39	0.736	0.968	5581	0.08956125	0.973
38361	Homo sapiens	GSM1022946	POLR2A	None	T Lymphocyte	Blood	38	0.7341	0.964	6984	0.1400275	0.975
38431	Homo sapiens	GSM1022950	POLR2A	None	T Lymphocyte	Blood	39	0.7477	0.97	6222	0.09659675	0.971
38433	Homo sapiens	GSM1022948	POLR2A	None	T Lymphocyte	Blood	39	0.7713	0.974	1407	0.03362775	0.9644
38454	Homo sapiens	GSM1022945	POLR2A	None	T Lymphocyte	Blood	39	0.7491	0.957	5196	0.079669	0.9732
47435	Homo sapiens	GSM1201946	REST	None	T Lymphocyte	Blood	37	0.6073	0.886	1840	0.0628475	0.916
44097	Homo sapiens	GSM1056935	RUNX1	None	T Lymphocyte	Blood	39	0.7136	0.886	1187	0.0181065	0.9504
53629	Homo sapiens	GSM1577746	STAT5B	None	T Lymphocyte	Blood	37	0.7536	0.767	8377	0.1459865	0.95
53630	Homo sapiens	GSM1577747	STAT5B	None	T Lymphocyte	Blood	37	0.7297	0.708	8462	0.1848495	0.9604
53631	Homo sapiens	GSM1577748	STAT5B	None	T Lymphocyte	Blood	38	0.6881	0.676	2727	0.07564975	0.804
5195	Homo sapiens	GSM630810	YY1	None	T Lymphocyte	Blood	20	0.5189	0.783	3788	0.119051698	0.9708

References

1. Becht, E. et al. Dimensionality reduction for visualizing single-cell data using UMAP. *Nat Biotechnol* (2018).
2. Ma, S. et al. Chromatin Potential Identified by Shared Single-Cell Profiling of RNA and Chromatin. *Cell* **183**, 1103-1116 e1120 (2020).
3. Hao, Y. et al. Integrated analysis of multimodal single-cell data. *Cell* **184**, 3573-3587 e3529 (2021).
4. Chen, S., Lake, B.B. & Zhang, K. High-throughput sequencing of the transcriptome and chromatin accessibility in the same cell. *Nat Biotechnol* **37**, 1452-1457 (2019).
5. Zhu, C. et al. An ultra high-throughput method for single-cell joint analysis of open chromatin and transcriptome. *Nat Struct Mol Biol* **26**, 1063-1070 (2019).
6. Stuart, T., Srivastava, A., Lareau, C. & Satija, R. Multimodal single-cell chromatin analysis with Signac. *bioRxiv*, 2020.2011.2009.373613 (2020).
7. Mei, S. et al. Cistrome Data Browser: a data portal for ChIP-Seq and chromatin accessibility data in human and mouse. *Nucleic Acids Res* **45**, D658-D662 (2017).
8. Zhang, Y. et al. Model-based analysis of ChIP-Seq (MACS). *Genome Biol* **9**, R137 (2008).